Antitumor Activity of NLG207 (Formerly CRLX101) in Combination with Enzalutamide in Preclinical Prostate Cancer Models

Keith T. Schmidt[1], Cindy H. Chau[1], Jonathan D. Strope[1], Alwin D.R. Huitema[2,3], Tristan M. Sissung[1], Douglas K. Price[1], and William D. Figg[1]

ABSTRACT

Effective treatments for patients with metastatic castration-resistant prostate cancer following disease progression on enzalutamide are currently an unmet clinical need. Simultaneous inhibition of the hypoxia-inducible factor (HIF)-1α and androgen receptor (AR) pathways has been previously shown to overcome enzalutamide resistance *in vitro*. Combination treatment with NLG207, a nanoparticle–drug conjugate of camptothecin and inhibitor of HIF-1α, and enzalutamide was evaluated in preclinical prostate cancer models of enzalutamide resistance. The effect of NLG207 and enzalutamide on average tumor volume and tumor re-growth after 3 weeks of treatment was evaluated *in vivo* using the subcutaneous 22Rv1 xenograft and castrated subcutaneous VCaP xenograft models. Correlative assessments of antitumor activity were evaluated *in vitro* using cell proliferation and qPCR assays. NLG207 8 mg/kg alone and in combination with enzalutamide reduced average tumor volume by 93% after 3 weeks of treatment ($P < 0.05$) in comparison with vehicle control in the subcutaneous 22Rv1 xenograft model. Notably, the addition of NLG207 also enhanced the efficacy of enzalutamide alone in the castrated subcutaneous VCaP xenograft model, decreasing the median rate of tumor growth by 51% ($P = 0.0001$) in comparison with enzalutamide alone. *In vitro* assessments of cell proliferation and gene expression further demonstrated antitumor activity via AR–HIF-1α crosstalk inhibition. Combination treatment with NLG207 and enzalutamide was shown to be effective in preclinical prostate cancer models of enzalutamide resistance. Clinical investigation of this treatment combination is ongoing (NCT03531827).

Introduction

Enzalutamide (ENZ), an androgen receptor antagonist (ARA), and abiraterone acetate, a CYP17 inhibitor, are current primary standard-of-care treatment options for patients with metastatic castration-resistant prostate cancer (mCRPC; ref. 1). Acquired resistance to these agents is inevitable, ultimately resulting in clinical disease progression and initiation of additional lines of therapy (2). Mechanisms of acquired resistance include alterations of DNA damage repair mechanisms, activation of alternative cell signaling pathways (e.g., PI3K, Wnt/β-catenin), and aberrations in androgen receptor (AR) activity (3). Notably, AR–full-length (AR-FL) overexpression and expression of AR splice variants (e.g., AR-V7) are commonly associated with disease progression following enzalutamide monotherapy (4–7). Recent clinical investigations often focus on combinatorial treatment approaches aimed to target one or multiple pathways of acquired resistance.

Intratumoral hypoxia serves an important role in prostate cancer aggressiveness and metastatic potential, as cells adapt to hypoxic environments via co-opting blood vessel formation and migrating toward vessels (8–11). Hypoxia-inducible factor (HIF)-1α, a transcription factor upregulated in response to hypoxia, is responsible for promoting tumor angiogenesis, anaerobic metabolism, immunity, adaptation, and invasion (11–13). Androgen deprivation can also contribute to prostate cancer cell adaptation to hypoxic environments, upregulating transcriptional activity of the AR (14, 15). Crosstalk between the HIF-1α and AR pathways has been suggested via a ternary complex comprising AR, HIF-1α, and β-catenin on androgen response elements of AR-target genes (16–18). Thus, targeting HIF-1α was hypothesized to downregulate AR-mediated gene expression and reduce prostate cancer cell proliferation. Our laboratory previously investigated the dual targeting of both axes via combination treatment of enzalutamide with HIF-1α inhibition in prostate cancer cells to define the molecular mechanisms by which HIF-1α inhibition potentiates anti-AR therapy in CRPC. HIF-1α inhibition, achieved via chetomin (disruptor of HIF-1α-p300 interactions) or siRNA silencing of HIF-1α, in combination with enzalutamide synergistically reduced AR-regulated and HIF-1α–mediated transcription, reduced VEGF protein expression, and inhibited cell growth (18). In 22Rv1 cells, a cell line with enzalutamide resistance mediated via androgen independence and significant AR splice variant expression (19–21), enzalutamide activity was significantly enhanced following HIF-1α inhibition (18).

In the current study, we further investigate this therapeutic approach by evaluating the combination treatment of enzalutamide with NLG207, formerly known as CRLX101. NLG207 is a nanoparticle–drug conjugate of camptothecin (CPT) designed to overcome the poor physicochemical properties associated with small-molecule camptothecin, while also using the enhanced permeation and retention effect to more optimally facilitate drug delivery to tumors (22, 23).

[1]Genitourinary Malignancies Branch, Center for Cancer Research, National Cancer Institute, National Institutes of Health, Bethesda, Maryland. [2]Department Pharmacy and Pharmacology, Netherlands Cancer Institute, Amsterdam, The Netherlands. [3]Department of Clinical Pharmacy, University Medical Center Utrecht, Utrecht University, Utrecht, The Netherlands.

Note: Supplementary data for this article are available at Molecular Cancer Therapeutics Online (http://mct.aacrjournals.org/).

Corresponding Author: William D. Figg, Clinical Pharmacology Program and Genitourinary Malignancies Branch, National Cancer Institute, 10 Center Drive, Bethesda, MD 20892. Phone: 240-760-6179; Fax: 240-858-3020; E-mail: figgw@helix.nih.gov

Mol Cancer Ther 2021;20:915–24

doi: 10.1158/1535-7163.MCT-20-0228

Camptothecins, potent inhibitors of topoisomerase I, have previously been shown to block the accumulation of HIF-1α and subsequently the expression of VEGF (24, 25). Studies with NLG207 have also demonstrated effective targeting of HIF-1α and inhibition of angiogenesis in models of ovarian cancer, breast cancer, and glioblastoma, either as monotherapy or in combination with bevacizumab (26–29). Thus, we assessed the antitumor activity of NLG207 in combination with enzalutamide in subcutaneous xenograft models of prostate cancer with clinically relevant mechanisms of acquired resistance to enzalutamide.

Materials and Methods

Cell culture

22Rv1 cells were maintained in phenol red-free RPMI-1640, and VCaP cells were maintained in DMEM, both supplemented with 10% FBS, 50 U/mL Penicillin, and 50 mg/mL Streptomycin. Both 22Rv1 and VCaP cells were purchased from the ATCC. The ATCC uses short tandem repeat profiling for testing and authentication of cell lines. Cells were thawed and sub-cultured per the ATCC recommendations, with cells designated for *in vitro* experiments cultured for fewer than 3 months and routinely screened for *Mycoplasma*. For *in vivo* experiments, cells were thawed directly from original ATCC vials and expanded until the sufficient amount of cells needed for inoculation to generate subcutaneous xenografts (4–7 passages).

Reagents

R1881 and S-(+)-Camptothecin were purchased from Millipore Sigma, enzalutamide was purchased from Selleck Chemicals, and NLG207 was provided by NewLink Genetics. All doses of NLG207 (mg) were measured using camptothecin equivalents, or the mass of camptothecin contained within the nanoparticle formulation.

Cell proliferation assays

22Rv1 and VCaP cells were seeded in 96-well plates in 100 μL 10% charcoal–dextran stripped (CDS) FBS supplemented phenol-red–free RPMI-1640 and DMEM (supplemented with 4 mmol/L L-gluatmine) medium, respectively. Cells were seeded at densities of 5,000 and 30,000 cells per well for 22Rv1 and VCaP, respectively. Following 24–48 hours incubation, cells were treated with the corresponding 10% CDS–FBS supplemented media containing 0.1 nmol/L R1881 and either DMSO control, camptothecin, NLG207, enzalutamide, CPT + ENZ, or NLG207 + ENZ (day 0). Cells were re-dosed on day 4 after treatment. Cell viability was measured on days 0, 3, 5, and 7 using the Cell Counting Kit-8 cell proliferation/cytotoxicity assay according to the manufacturer's instructions (Dojindo), and absorbance was read at 450 nm using a SpectraMax iD3 fluorescence plate reader (Molecular Devices).

Semiquantitative real-time PCR

VCaP cells were plated at a density of 800,000 cells per well in a 6-well dish in phenol red-free DMEM media supplemented with 10% CDS–FBS for 48 hours. Cells were then treated with 10% CDS–FBS supplemented media with or without 0.1 nmol/L R1881 and combinations of DMSO control, 500 nmol/L camptothecin, 500 nmol/L NLG207, and/or 500 nmol/L enzalutamide for 24 hours. Total RNA was extracted using the RNAeasy mini kit (Qiagen) per the manufacturer's protocol. Purified RNA (~0.24 μg) was reverse transcribed via 30-μL cDNA synthesis reaction using the SuperScript III First Strand Synthesis System (Invitrogen) per the manufacturer's protocol.

cDNA synthesis products were amplified in triplicate with forward and reverse primers: KLK3 (Hs02576345_m1, Applied Biosystems), ERG (Hs01554629_m1, Applied Biosystems), VEGFA (Hs00900055_m1, Applied Biosystems), LDHA (Hs00855332_g1, Applied Biosystems), and ACTB (Hs99999903_m1, Applied Biosystems). Custom primers (Applied Biosystems) for AR-FL and AR-V7 were previously described (30, 31). The specificity of these primers were evaluated in PC3, 22Rv1, and VCaP cells, and compared with LNCaP95 cells. All other primers used were commercially available and previously validated (18, 32).

Two microliters of cDNA per sample was mixed with 1 μL forward and reverse primers, 7 μL water, and 10 μL TaqMan Gene Expression Master Mix (Applied Biosystems) for a total of 20 μL. Semiquantitative real-time PCR (qPCR) was performed using an Applied Biosystems StepOnePlus Real-Time PCR system with StepOne Software. All qPCR reactions were run in triplicate using the standard TaqMan protocol for 40 cycles, with use of β-actin (ACTB) as the reference housekeeping gene. Fold-change in RNA levels was calculated using the $\Delta\Delta C_t$ method. For AR-FL and AR-V7 primer validation, the same qPCR reaction conditions were used for 30 cycles. PCR products were mixed with DNA gel loading dye (6x; Thermo Fisher Scientific), applied to 4%–20% TBE gels (Invitrogen) and stained with SYBR Green (Invitrogen). The GeneRuler 50 bp DNA Ladder (Thermo Fisher Scientific) was used as a size standard, and PCR fragments were visualized using an Odyssey Fc Imager (LI-COR Biosciences; Supplementary Fig. S1).

Animal care

All animals were housed in a pathogen-free facility of the National Cancer Institute, which is accredited by the Association for Assessment and Accreditation of Laboratory Animal Care (AAALAC) International and follows the Public Health Service (PHS) Policy for the Care and Use of Laboratory Animals. Animal care was provided in accordance with the Guide for the Care and Use of Laboratory Animals. The study protocol was approved by the NCI Animal Care and Use Committee (ACUC).

22Rv1 subcutaneous xenografts

Approximately 5×10^6 22Rv1 cells (suspended in DPBS) were subcutaneously injected into the rear flank of 6-week-old, male, SCID mice. Tumors were grown to a volume greater than 50 mm^3 before stratification into treatment groups (Study 1: $n = 4$–5; Study 2: $n = 9$–10): vehicle control, enzalutamide only (25 mg/kg in 50:50 PEG-400:Tween 80 via daily oral gavage), NLG207 4 or 8 mg/kg (in DPBS via weekly intraperitoneal injection) ± enzalutamide. Mice were treated for 3 weeks, with weight measurements daily and tumor volume measurements three times weekly, using the formula $V = (L \times W^2)/2$ (length corresponding to longer dimension of tumor). Following 3 weeks of treatment in the first study, the mice were euthanized and tumors were harvested to obtain final weight and volume [using $L \times W \times H \times (\pi/6)$] measurements. In the second study, mice were followed after treatment course completion three times weekly until tumors ulcerated or reached >2 cm in one direction, prompting removal from study and euthanasia per NCI ACUC guidance. Mice with >20% reduction in body weight were removed and censored.

Castrated *VCaP* subcutaneous xenograft

Approximately 2.5×10^6 VCaP cells (suspended in 50:50 DPBS: Matrigel) were injected into the rear flank of 6-week-old, male, SCID mice. When the average tumor volume reached approximately 200 mm^3 (measured via $V = (L \times W^2)/2$) the mice were castrated

(removal of the testes facilitated via scrotal incision and vaginal tunic access) under isoflurane anesthesia. The mice were followed up post-surgically for 10 days, and tumors were allowed to regrow to an average volume of approximately 200 mm^3. The mice were then stratified on the basis of tumor volume into 4 treatment groups ($n = 9–10$): Vehicle control, enzalutamide 25 mg/kg daily, NLG207 8 mg/kg once weekly, and combination. Mice were treated for 3 weeks, with tumor measurements obtained 3 times weekly and body weight measurements collected daily. Following 3 weeks of treatment, animals were monitored for tumor size and body weight three times weekly. Mice were removed from study if tumors reached >2 cm in any dimension per NCI ACUC guidance; mice with >20% reduction in body weight were removed from study and censored. Following 6 weeks after treatment, all remaining animals were euthanized.

Statistical analyses

Unpaired *t* tests were used for between group comparisons of cell proliferation. Tumor growth curves were reported as mean tumor volumes ± SEM and mean percentage change in tumor volume (start of treatment as baseline) ± SEM for the 22Rv1 and VCaP xenograft models, respectively. Body weight curves were reported as mean body weight ± SEM. Comparisons of average tumor volumes, average tumor volume change, average tumor weights, and fold change in gene expression at specified timepoints were made using Mann–Whitney tests. The Kaplan–Meier method was used to assess median survival (i.e., time to tumor >2 cm in one dimension) and progression-free survival (i.e., tumor doubling in size from baseline) for the 22Rv1 and VCaP xenograft models, respectively. Log-rank (Mantel-Cox) tests were used to determine statistical significance of survival differences between treatment groups. Statistical analyses were performed using GraphPad Prism 8 ($P < 0.05$ was used as the threshold for statistical significance).

Results

Enhanced activity of enzalutamide in combination *with NLG207 in 22Rv1* cells

First, the effect of NLG207 and enzalutamide on the growth of 22Rv1 cells was evaluated *in vitro*. The approximate IC_{50} values for NLG207 and camptothecin in 22Rv1 cells were 10 and 5 nmol/L, respectively (Supplementary Fig. S2A); camptothecin was included to confirm activity was associated with the camptothecin component of NLG207. The IC_{50} value for enzalutamide in 22Rv1 cells was 1 μmol/L, consistent with previous literature (21). Enzalutamide, NLG207, and camptothecin each significantly downregulated cell proliferation in the presence of 0.1 nmol/L R1881 by 5 days of treatment (**Fig. 1A** and **B**). Treatment with NLG207 or camptothecin in combination with enzalutamide in 22Rv1 cells enhanced the effect of enzalutamide alone by 58.3% and 59.9% by day 7, respectively ($P < 0.0001$), after treatment initiation. The enhancement of enzalutamide antitumor activity via NLG207 co-treatment mirrored previous data with siHIF + ENZ in 22Rv1 cells (18).

Efficacy of NLG207 and enzalutamide in 22Rv1 xenograft model

The efficacy of NLG207 and enzalutamide was first evaluated via analysis of tumor volume reduction following 3 weeks of treatment using the subcutaneous 22Rv1 xenograft model, a model previously used by Liu and colleagues (33, 34). The 4 and 8 mg/kg doses of NLG207 were derived from prior xenograft studies by Pham and colleagues (28, 29). Comparisons of daily tumor measurements collected on study showed NLG207 8 mg/kg ± enzalutamide and NLG207 4 mg/kg ± enzalutamide significantly reduced average tumor volume compared with vehicle control by day 7 and 11 after treatment, respectively ($P < 0.05$; **Fig. 2A**). All groups treated with NLG207 had significant reductions in tumor volume compared with enzalutamide alone by day 14 ($P < 0.05$). In harvested tumors, average volume and weight comparisons between vehicle control and enzalutamide alone were consistent with enzalutamide resistance ($P > 0.05$; **Fig. 2B–D**). All NLG207 treated groups had significantly reduced average harvested tumor weights compared with either vehicle control or enzalutamide alone ($P < 0.05$). Relative to vehicle control, treatment with NLG207 8 mg/kg + enzalutamide reduced harvested tumor volume by 93%, and NLG207 4 mg/kg + enzalutamide, by comparison, only showed an 81% reduction ($P < 0.05$). On the basis of these data, we used the 8 mg/kg dose of NLG207 for future xenograft studies. An additional xenograft study assessing tumor re-growth (an endpoint commonly used to evaluate NLG207 efficacy; ref. 35) following 3 weeks of treatment with 8 mg/kg NLG207 and enzalutamide confirmed these findings while demonstrating significantly increased survival in mice treated with NLG207 (Supplementary Fig. S3).

Toxicity was evaluated via average body weight measurements, taken daily during treatment and three times weekly after treatment (**Fig. 2E**). Two mice were removed from both studies due to >20% reduction in body weight: One mouse receiving NLG207 8 mg/kg and one mouse receiving NLG207 8 mg/kg + enzalutamide. Trends of decreased average body weight were seen in groups receiving NLG207 compared with either vehicle control or enzalutamide alone.

Effect of NLG207 on cell proliferation and gene expression in VCaP cells

The antitumor activity of NLG207 + ENZ was further evaluated in the VCaP cell line. Unlike 22Rv1 cells, which express AR-V7 and other splice variants via AR intragenic rearrangement, VCaP cells express AR-V7 via significantly increased AR gene transcript generation (19, 20, 33, 36). VCaP cells also overexpress AR-FL and harbor the TMPRSS2–ERG fusion, relevant characteristics in advanced mCRPC that are not present in 22Rv1 cells (36). The approximate *in vitro* IC_{50} values were 500 nmol/L for NLG207 and 500 nmol/L for camptothecin in VCaP cells (Supplementary Fig. S2B), a 50- and 100-fold decrease in potency, respectively, compared with 22Rv1 cells. In VCaP cells, the IC_{50} value for enzalutamide was 500 nmol/L, a 2-fold increase in potency compared with 22Rv1 and similar to the previously reported value (37). Enzalutamide, NLG207, and camptothecin each significantly downregulated cell proliferation in the presence of 0.1 nmol/L R1881 by 3 days after treatment (**Fig. 3A** and **B**). Treatment of NLG207 or camptothecin in combination with enzalutamide enhanced cell growth inhibition of enzalutamide alone by 60% and 61.5%, respectively, by day 7 ($P < 0.0001$).

We next examined the effect of drug treatments on changes in mRNA expression of AR pathway genes in VCaP cells treated with 0.1 nmol/L R1881 *in vitro*. Trends in AR-associated gene expression in response to androgen stimulation with or without enzalutamide (**Fig. 4**) were consistent with prior literature (36, 38–40). Androgen stimulation or NLG207 alone preferentially suppressed AR-V7 versus AR-FL mRNA expression whereas this effect is blunted following enzalutamide treatment (**Fig. 4A** and **B**). Treatment with 500 nmol/L NLG207 alone had a more robust effect on AR-FL/AR-V7 compared with androgen stimulation. The addition of NLG207 to enzalutamide treatment more effectively attenuated AR-V7 expression (2.9-fold compared with enzalutamide alone, $P < 0.0001$). Downstream AR target genes, KLK3 and ERG, were significantly downregulated following combination treatment, with 2.8- and 4.6-fold reductions

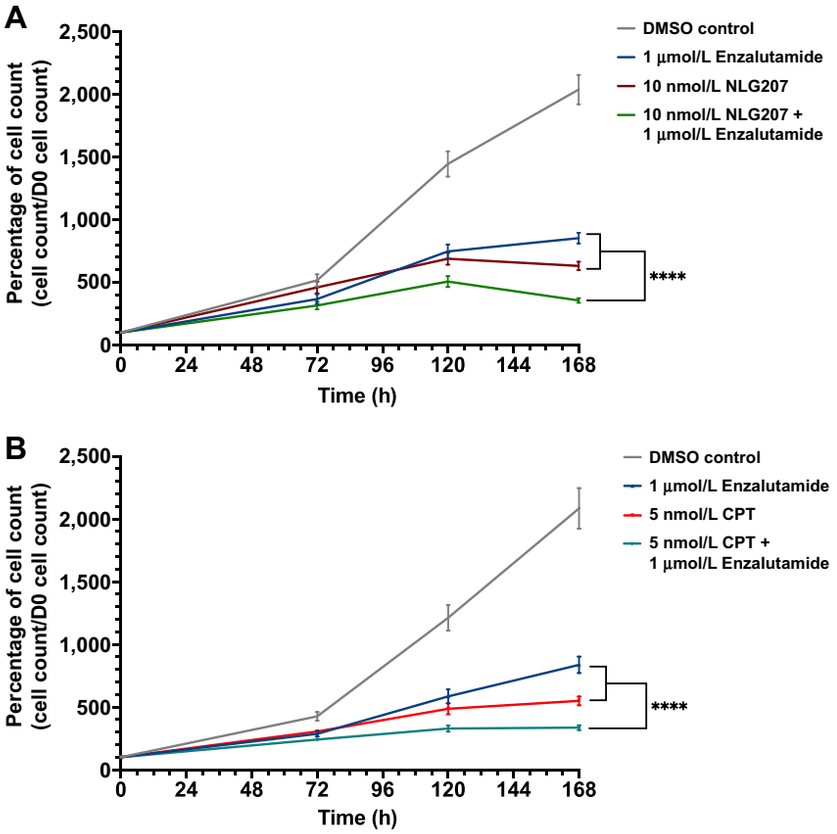

Figure 1.

Effect of NLG207, camptothecin, and enzalutamide on cell proliferation of 22Rv1 cells. Growth of 22Rv1 cells in media containing 0.1 nmol/L R1881 with or without 1 μmol/L enzalutamide was evaluated over 168 hours following treatment with 10 nmol/L NLG207 (**A**) or 5 nmol/L camptothecin (**B**). Cell viability was determined using the Cell Counting Kit-8 cell proliferation/cytotoxicity assay at the indicated time points. The result is representative of three independent experiments. Statistical significance between groups by day 7 is denoted: ****, $P < 0.0001$.

observed compared with enzalutamide alone, respectively (**Fig. 4C** and **D**; $P < 0.0001$). Treatment with 500 nmol/L camptothecin instead of NLG207 resulted in similar but more robust changes in gene expression, likely explained via nanoparticle release kinetics (Supplementary Fig. S4). VEGFA and LDHA, HIF-1α downstream target genes, were also downregulated following treatment with NLG207 or camptothecin (Supplementary Fig. S5); combination CPT + ENZ treatment resulted in 1.7- and 2.5-fold reductions in VEGFA and LDHA, respectively, when compared with enzalutamide alone ($P < 0.0001$). Similar findings were noted in our prior study examining the effect of combination of chetomin and enzalutamide on target gene expression (18).

NLG207 enhances enzalutamide activity in castrated *VCaP*-xenografted mice

Finally, we investigated the efficacy of NLG207 8 mg/kg + enzalutamide 25 mg/kg in the castrated VCaP subcutaneous xenograft model. Cai and colleagues (41) first described the effects of castration on pre-established VCaP-xenografted tumors, demonstrating that AR activity and ERG expression are restored following castration, with marked increases in AR mRNA expression. Evaluation of NLG207 and enzalutamide antitumor activity in the castrated VCaP subcutaneous xenograft model was implemented similarly to recent preclinical evaluations of second-generation AR antagonist-based treatments (37, 42). The average percentage of change in tumor volume from baseline per treatment group is summarized in **Fig. 5A**. The NLG207-treated groups had significant reductions in tumor volume compared with vehicle control or enzalutamide by day 10 after treatment initiation ($P < 0.05$). NLG207 + ENZ was significantly better than NLG207 alone ($P \leq 0.05$) throughout several timepoints after treatment initiation, including days 8 (after second NLG207 injection), 22 (end of treatment [EOT]), and 36 (2 weeks after EOT). Although the effect of NLG207 with enzalutamide provided a persistent reduction in tumor growth in comparison with NLG207 alone well after treatment cessation, the effect of enzalutamide in comparison with vehicle control dissipated before the end of treatment. The median progression-free survival (i.e., tumor doubling time) was different between the vehicle control and enzalutamide alone groups (**Fig. 5B**), both reached before EOT (13 and 20 days, respectively; $P < 0.05$); the antitumor effect of enzalutamide alone was consistent with prior studies describing minimal sensitivity to the agent in the castrated VCaP xenograft model (37, 42). The median progression-free survival of the NLG207 8 mg/kg + enzalutamide treatment group was significantly improved in comparison with NLG207 8 mg/kg alone (31 and 41 days, respectively, $P < 0.05$). Importantly, the addition of NLG207 to enzalutamide treatment reduced the median rate of tumor growth (assessed via progression-free survival) by 51% in comparison with enzalutamide alone ($P = 0.0001$).

Castration and NLG207 treatment were associated with declines in average body weight measurements (**Fig. 5C**). A brief reduction in average body weight was observed during after castration follow-up, with weight stabilizing close to baseline before treatment initiation. NLG207 alone was the least well tolerated, with average body weight nadirs occurring 3 days after intraperitoneal injection; enzalutamide appeared to negate this effect, as the average body weight nadirs of mice treated with NLG207 + ENZ were smaller by comparison. Three mice were euthanized following >20% body weight reduction: One during after castration follow-up, one from the NLG207 alone group (day 7 of

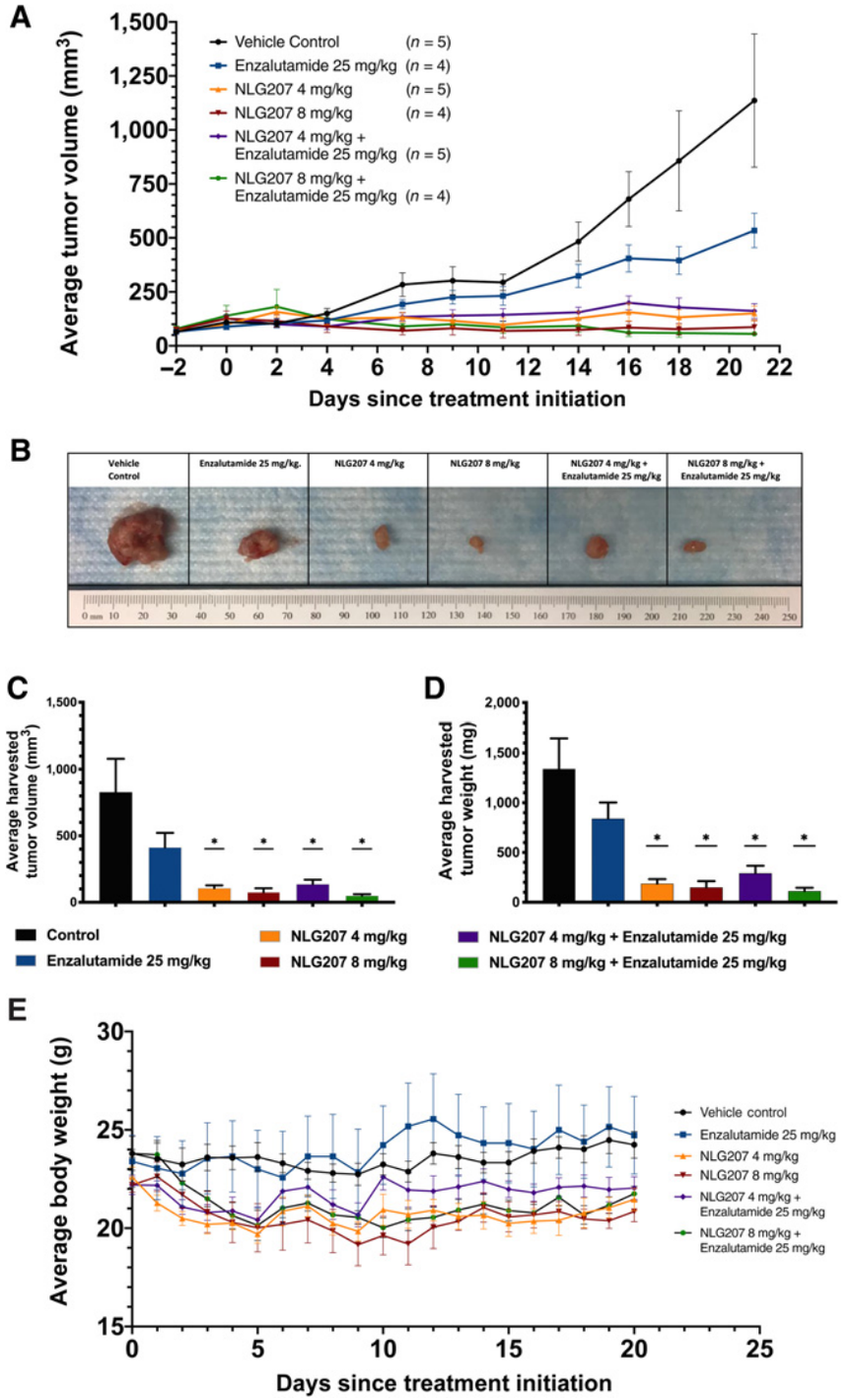

Figure 2.

Efficacy of NLG207 and enzalutamide in subcutaneous 22Rv1 xenografts after 3 weeks of treatment. Mice with subcutaneous 22Rv1 xenografts were treated for 3 weeks with the specified doses of vehicle controls, enzalutamide and/or NLG207, and euthanized at the completion of treatment. Average tumor volume measurements collected are plotted during the course of the study (**A**). Tumors, harvested following 3 weeks of treatment, were compared, as shown via photograph with one tumor per group (**B**), average tumor volume (**C**) and average tumor weight (**D**) at time of harvest; statistical comparisons with vehicle control above each treatment group are denoted: *, $P < 0.05$. Daily average body weight measurements collected are summarized over the course of the study (**E**).

treatment), and one from the NLG207 + ENZ group (day 10 of treatment).

Discussion

The use of NLG207 in combination with enzalutamide presented a reasonable approach to downregulate AR–HIF crosstalk, as suggested by prior study in enzalutamide-resistant 22Rv1 cells (18). First, NLG207 was shown to be a potent inhibitor of tumor growth, both as monotherapy and in combination with enzalutamide, in the 22Rv1 xenograft model. The addition of NLG207 was then shown to potentiate the anti-AR effects of enzalutamide in the castrated VCaP xenograft model, which exhibits AR amplification and splice variant expression, two relevant mechanisms of AR-mediated acquired resistance to enzalutamide. The combination treatment demonstrated robust activity in both the 22Rv1 and castrated VCaP xenograft

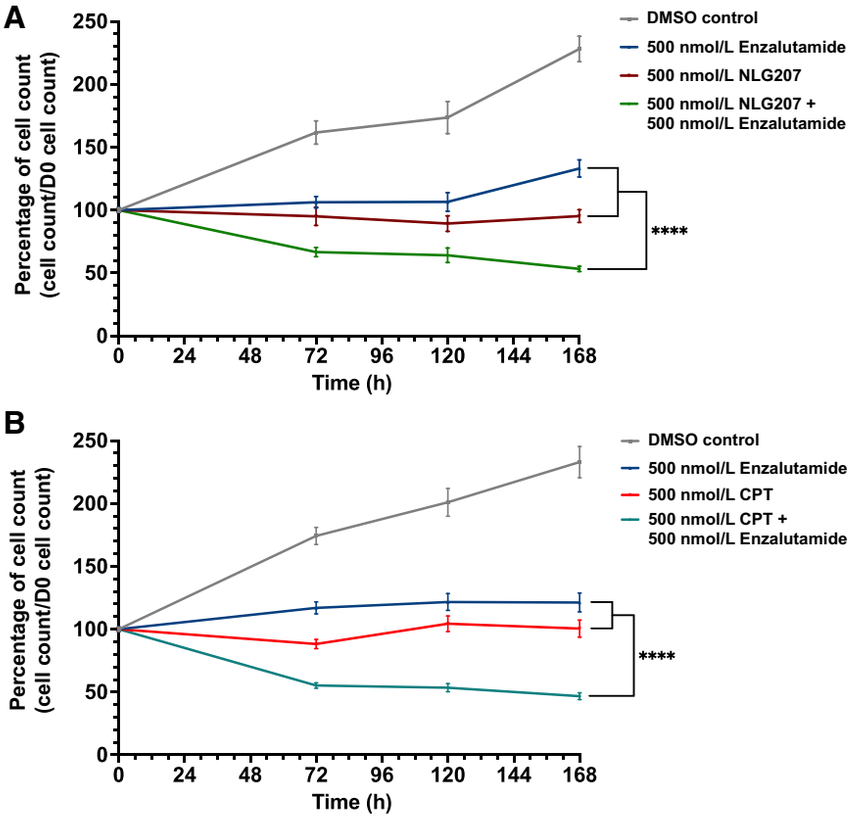

Figure 3.

Effect of NLG207, camptothecin, and enzalutamide on cell proliferation of VCaP cells. Growth of VCaP cells in media containing 0.1 nmol/L R1881 with or without 500 nmol/L enzalutamide was evaluated over 168 hours following treatment with 500 nmol/L NLG207 (**A**) or 500 nmol/L camptothecin (**B**). Cell viability was determined using the Cell Counting Kit-8 cell proliferation/cytotoxicity assay at the indicated time points. The result is representative of three independent experiments. Statistical significance between groups by day 7 is denoted: ****, $P < 0.0001$.

models, with evidence supporting the downregulation of AR pathway–gene expression in VCaP cells, including AR-FL, AR-V7 and downstream targets.

Camptothecin, the "payload" of the β-cyclodextrin-polyethylene glycol co-polymer NLG207 formulation and a potent topoisomerase I (TOP1) inhibitor (22), has been previously shown to exhibit indirect effects on HIF-1α and AR activity, both dependent on anti-TOP1 activity. Rapisarda and colleagues (43) first demonstrated the effect of topotecan (TPT), a camptothecin derivative, on HIF-1α accumulation if given at low, persistent doses, which was dependent upon TOP1 inhibition. TOP1 was previously shown to co-occupy enhancer binding sites with NKX3.1 to regulate AR transcription, with the catalytic activity of TOP1 to nick DNA important for AR-regulated enhancer activation (44). A similar β-cyclodextrin nanosponge formulation of camptothecin (CN-CPT) was previously shown to exert activity against TOP1 via the upregulation of γ-H2AX, a marker of DNA damage, in AR-null PC3 and DU-145 cells; with increased doses, similar effects on γ-H2AX were seen in the AR T878A variant expressing LNCaP cell line, while also accompanied by depletion of the AR (45). Extension of these studies with CN-CPT in DU-145 and PC-3 cells showed inhibition of adhesion and migration of tumor cells while decreasing STAT3 phosphorylation, supporting beneficial anti-angiogenic activity when coupled with *in vivo* antitumor activity in PC3 xenografted mice (46). NLG207 was previously shown to induce γ-H2AX formation and decrease HIF-1α levels in rectal cancer cells, and downregulate HIF-1α in breast cancer tumor xenografts (27, 47). Evaluation of clinical tumor specimens via IHC following NLG207 treatment demonstrated both activity against Ki-67 and downstream targets of HIF-1α (CAIX and VEGFA), while decreasing TOP1 expression (48). Finally, TOP1 was shown reside on HIF-1α, AR-FL, and AR-V7 mRNA; co-treatment with TPT and enzalutamide in hypoxic 22Rv1 cells resulted in HIF-1α knockdown, reduced AR-V7 nuclear localization, and synergistic dose response (49). The summation of these data highlights the multifaceted nature of camptothecin antitumor activity stemming from potent TOP1 inhibition.

Using validated AR species-specific primers (30, 31), our *in vitro* analyses demonstrated decreases in AR-FL and notably AR-V7 mRNA expression in VCaP cells following treatment with NLG207. Furthermore, NLG207 enhanced enzalutamide's ability to downregulate the mRNA expression of KLK3 and ERG, both downstream AR-targets, mirroring previous data shown with chetomin and enzalutamide treatment (18). Downstream targets of HIF-1α signaling, VEGFA and LDHA, were also downregulated in response to NLG207 and camptothecin under normoxia. The impact of treatment VEGFA and LDHA mRNA expression was not evaluated in the context of hypoxia and subsequent HIF-1α accumulation, a limitation of the present study (18). In addition, we lacked sufficient tumor tissue to compare *in vivo* gene and protein expression of relevant pharmacodynamic biomarkers after treatment due to our xenograft study endpoint selection (33, 35). Given the robust suppression of NLG207 on AR-FL/AR-V7, whether NLG207 has an effect on the heterodimerization of AR-FL with AR-V7 remains to be determined; however, preliminary evidence has been suggested by TPT treatment in 22Rv1 cells (50).

NLG207 was highly potent in both the 22Rv1 and castrated VCaP subcutaneous xenograft models. Prior subcutaneous xenograft models, including colorectal models evaluating NLG207 treatment in combination with 5-FU and oxaliplatin, have similarly shown significant reductions in tumor volume followed by decreased rates of tumor re-growth (47); subcutaneous xenograft studies evaluating NLG207 have limited dosing frequency and have established efficacy

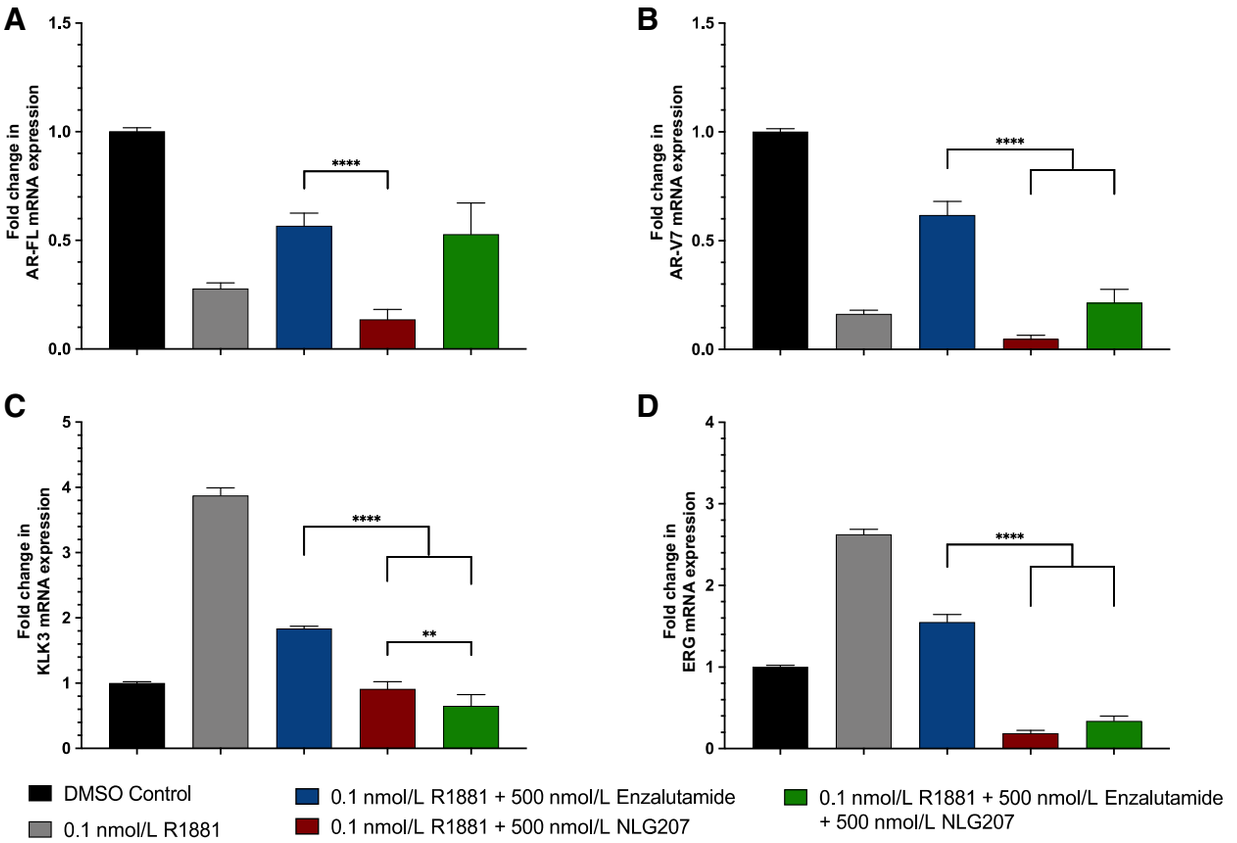

Figure 4.

Effect of NLG207 and enzalutamide on mRNA expression of relevant AR pathway–associated genes in VCaP cells. The fold change in mRNA expression of AR-FL (**A**), AR-V7 (**B**), KLK3 (**C**), ERG (**D**) following 24 hours of treatment with combinations of R1881, enzalutamide and NLG207 compared with cells in 10% CDS–FBS supplemented media. Results are representative of three independent experiments. Significance of indicated comparisons is denoted: **, $P < 0.01$; ****, $P < 0.0001$.

on the basis of re-growth rates (35). Unsurprisingly, 4 and 8 mg/kg NLG207 with or without enzalutamide significantly decreased tumor growth in the 22Rv1 model following just 3 weeks of treatment, although a dose-dependent effect was not observed in this prostate cancer model because of the sensitivity of 22Rv1 cells to NLG207. In the castrated VCaP xenograft model, similar reductions in tumor growth were observed after 3 weeks of treatment with NLG207 8 mg/kg, with enhanced activity of the combination in comparison with both NLG207 or enzalutamide alone at the end of treatment and 2 weeks post-end of treatment. Though the VCaP model does display some enzalutamide sensitivity from days 13 through 17, the effect dissipates before treatment cessation to indicate enzalutamide resistance, a finding similar to previous literature (51). With the addition of NLG207, enzalutamide has sustained antitumor effect long after treatment cessation, increasing the tumor doubling time by 20 days. These findings when coupled with *in vitro* data point toward both the potency of NLG207 to TOP1 inhibition and sustained reduction of tumor growth driven by indirect activity of camptothecin on the AR pathway.

Our *in vitro* analysis also demonstrated a 50-fold increase in the potency of NLG207 in 22Rv1 cells when compared with VCaP cells. The absence of a measurable effect of combination treatment versus NLG207 alone in 22Rv1 xenografts as opposed to VCaP xenografts further demonstrated this significant potency difference. Upregulation of ERG expression, a transcription factor of the ETS family promoted via the TMPRSS2–ERG fusion, is present in VCaP cells but not 22Rv1 cells (52). In addition to its effects on tumor cell invasiveness and proliferation (53), ERG has been implicated to disrupt the interaction of topoisomerase I and DNA-PKcs, which regulates the cellular response of camptothecin independently of DNA repair (54). A comparison of camptothecin sensitivity between VCaP and DU-145, the latter cell line with similar levels of ERG expression with that of 22Rv1 (52), demonstrated a >100-fold difference in potency to camptothecin (54), a near identical finding to our analysis of IC_{50} concentrations of camptothecin in VCaP and 22Rv1 cells. These data suggest the role of reduced ERG expression to significantly enhance the potency of NLG207. Interestingly, our findings show that camptothecin can decrease ERG mRNA expression in VCaP cells and another study implicates enhanced responses to enzalutamide associated with ERG expression in VCaP cells (55); despite the latter finding, recent data have suggested TMPRSS2–ERG to not be a predictive biomarker of enzalutamide efficacy in chemo-naïve patients with mCRPC in the first-line setting (56). Future investigations of ERG expression are necessary to better understand camptothecin sensitivity in prostate cancer cells and the role of TMPRSS2–ERG as a predictive biomarker of clinical outcomes following enzalutamide treatment.

In addition to ERG expression, the expression profile of the AR appears to be important to explain the sustained enhancement of

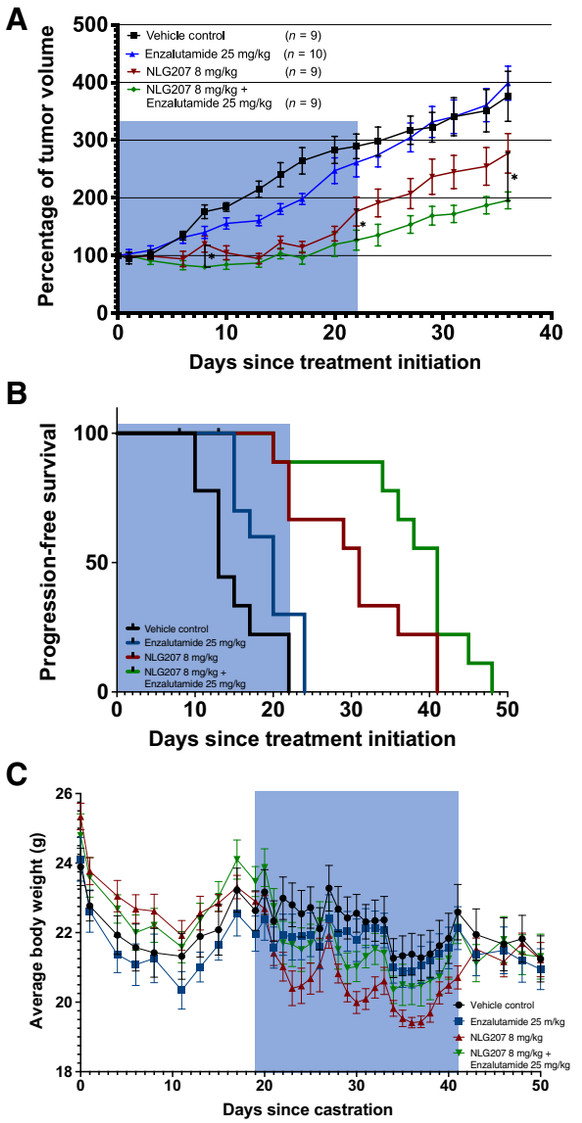

Figure 5.

Efficacy of NLG207 and enzalutamide in castrated subcutaneous VCaP-xenografted mice. Castrated mice with subcutaneous VCaP xenografts were treated for 3 weeks with specified doses of vehicle control, enzalutamide, and/or NLG207, then monitored for tumor re-growth. Average percentage of change in tumor volume measurements (baseline at the start of treatment) through day 36 after treatment initiation are summarized, with statistical significance of comparisons at specified time points denoted: *, $P \le 0.05$ (**A**). Kaplan–Meier survival analysis progression-free survival (progression indicated when a tumor doubled in size) for each treatment group (**B**). Mice were censored if treatment resulted in >20% reduction in body weight. Average body weight measurements per treatment group collected following castration through 10 days after drug treatment (**C**). The blue shading indicates the time frame for on-study drug treatment.

enzalutamide activity when combined with NLG207 treatment in VCaP xenografts. Camptothecin significantly reduced both AR-FL and AR-V7 mRNA expressions in the present study, as well as AR mRNA expression in prior studies with LNCaP cells (57, 58). Selective AR-variant knockdown has been previously shown to restore enzalutamide activity via AR-FL, or androgen-dependent, signaling in 22Rv1 cells (21); both the enhanced potency of NLG207 and potentially complete pan-AR variant inhibition limited our ability to ascertain a true effect of enzalutamide in 22Rv1 xenografts. However, AR-FL overexpression found in VCaP cells coupled with decreased potency of NLG207 may indicate incomplete suppression of AR-FL with NLG207 alone, enabling the re-sensitization to enzalutamide with lower intracellular concentrations of AR-FL. In a similar study, JQ1, a BET bromodomain inhibitor–targeting AR activity, also significantly downregulated AR-FL and AR-V7 transcription and enhanced the tumor growth inhibition of enzalutamide in the castrated VCaP xenograft model (42); combination of NLG207 and enzalutamide reduced tumor volume below baseline measurement, an effect not seen with JQ1 and enzalutamide (42). In addition, when compared with a previous study that assessed niclosamide, an agent that specifically promotes AR-V7 degradation, in the subcutaneous 22Rv1 xenograft model (33), the antitumor effect of NLG207 appears more potent. The inhibition of AR-FL and AR-V7 from the treatment combination will be further addressed in future biomarker-directed studies derived from the ongoing clinical investigation in patients with advanced mCRPC (NCT03531827).

Inhibition of AR-V7 expression appears to impact body weight for both xenograft models. Weight loss has been associated with NLG207 in prior reports in the literature (28). Interestingly, NLG207 and enzalutamide combination therapy appeared to have a weight-sparing effect, most notably in the castrated VCaP xenograft model. In the 22Rv1 xenografted mice, a similar weight-sparing effect was also implicated with 4 mg/kg doses of NLG207, but not the 8 mg/kg dose. The expression of AR-V7 has been previously shown to restore AR-mediated lipid biosynthesis via study of 22Rv1 and VCaP cells *in vitro* and *in vivo* (59). Increased AR-V7 mRNA expression following combination treatment in comparison with NLG207 alone, as shown via our *in vitro* data, may explain the weight-sparing effect observed in these models.

In conclusion, NLG207 in combination with enzalutamide had significant antitumor activity in two different preclinical prostate cancer models harboring clinically relevant mechanisms of enzalutamide resistance. AR-V7 expression, a potentially attractive predictive biomarker (4), is ultimately a result of two diverse oncogenic mechanisms driving enzalutamide resistance. AR amplification mediated via AR copy-number gain, modeled using VCaP cells (36, 41), has been well characterized in the context of disease progression on enzalutamide in numerous clinical studies (5–7). Constitutively active splice variant generation via AR intragenic gene rearrangement, modeled using 22Rv1 cells (19, 21), has recently been characterized in clinical CRPC tumors following enzalutamide treatment; intriguingly, AR gene rearrangements were not only shown to generate diverse AR-V species, but to also correlate with AR overexpression in the context of AR amplification (20). Our data indicate relevant downregulation of AR-FL and AR-V7 expression via a TOP1 inhibition-dependent mechanism facilitated by NLG207, enhancing the efficacy of enzalutamide. Antitumor activity of NLG207 and enzalutamide was demonstrated in both prostate cancer models of AR amplification and AR intragenic rearrangement, suggesting the potential of the treatment combination to effectively target tumors with heterogeneous mechanisms of enzalutamide resistance. In addition, the treatment combination was effective in the presence of the TMPRSS2–ERG fusion, a tumor characteristic present in nearly half of advanced prostate cancer cases in North America (60). Clinical investigation of this treatment combination to confirm antitumor activity in patients with mCRPC following disease progression on enzalutamide is currently ongoing (NCT03531827).

Authors' Disclosures

No disclosures were reported.

Disclaimer

The content of this publication does not necessarily reflect the views or policies of the Department of Health and Human Services, nor does mention of trade names, commercial products, or organization imply endorsement by the U.S. Government.

Authors' Contributions

K.T. Schmidt: Conceptualization, data curation, software, formal analysis, investigation, visualization, methodology, writing–original draft, project administration, writing–review and editing. **C.H. Chau:** Conceptualization, formal analysis, supervision, validation, investigation, visualization, methodology, writing–original draft, writing–review and editing. **J.D. Strope:** Data curation, investigation, methodology, project administration. **A.D.R. Huitema:** Conceptualization, supervision, writing–review and editing. **T.M. Sissung:** Formal analysis, supervision, investigation, methodology, writing–review and editing. **D.K. Price:** Resources, supervision, investigation, methodology, writing–review and editing. **W.D. Figg:** Conceptualization, resources, supervision, funding acquisition, investigation, writing–original draft, project administration, writing–review and editing.

Acknowledgments

This work was supported by the Intramural Research Program of the Center for Cancer Research, National Cancer Institute, National Institutes of Health (ZIA BC 010547).

The costs of publication of this article were defrayed in part by the payment of page charges. This article must therefore be hereby marked *advertisement* in accordance with 18 U.S.C. Section 1734 solely to indicate this fact.

Received March 25, 2020; revised June 6, 2020; accepted February 11, 2021; published first February 25, 2021.

References

1. Teo MY, Rathkopf DE, Kantoff P. Treatment of advanced prostate cancer. Annu Rev Med 2019;70:479–99.
2. Nakazawa M, Paller C, Kyprianou N. Mechanisms of therapeutic resistance in prostate cancer. Curr Oncol Rep 2017;19:13.
3. Robinson D, Van Allen EM, Wu Yi-Mi, Schultz N, Lonigro RJ, Mosquera J-M, et al. Integrative clinical genomics of advanced prostate cancer. Cell 2015;161:1215–28.
4. Antonarakis ES, Lu C, Wang H, Luber B, Nakazawa M, Roeser JC, et al. AR-V7 and resistance to enzalutamide and abiraterone in prostate cancer. N Engl J Med 2014;371:1028–38.
5. Annala M, Vandekerkhove G, Khalaf D, Taavitsainen S, Beja K, Warner EW, et al. Circulating tumor DNA genomics correlate with resistance to abiraterone and enzalutamide in prostate cancer. Cancer Discov 2018;8:444–57.
6. Azad AA, Volik SV, Wyatt AW, Haegert A, Le Bihan S, Bell RH, et al. Androgen receptor gene aberrations in circulating cell-free DNA: biomarkers of therapeutic resistance in castration-resistant prostate cancer. Clin Cancer Res 2015;21:2315–24.
7. Wyatt AW, Azad AA, Volik SV, Annala M, Beja K, McConeghy B, et al. Genomic alterations in cell-free DNA and enzalutamide resistance in castration-resistant prostate cancer. JAMA Oncol 2016;2:1598–606.
8. Bharti SK, Kakkad S, Danhier P, Wildes F, Penet M-F, Krishnamachary B, et al. Hypoxia patterns in primary and metastatic prostate cancer environments. Neoplasia 2019;21:239–46.
9. Fraga A, Ribeiro R, Principe P, Lopes C, Medeiros R. Hypoxia and prostate cancer aggressiveness: a tale with many endings. Clin Genitourin Cancer 2015;13:295–301.
10. Stewart GD, Ross JA, McLaren DB, Parker CC, Habib FK, Riddick AC. The relevance of a hypoxic tumour microenvironment in prostate cancer. BJU Int 2010;105:8–13.
11. Schito L, Semenza GL. Hypoxia-inducible factors: master regulators of cancer progression. Trends Cancer 2016;2:758–70.
12. Semenza GL. Defining the role of hypoxia-inducible factor 1 in cancer biology and therapeutics. Oncogene 2010;29:625–34.
13. Greer SN, Metcalf JL, Wang Y, Ohh M. The updated biology of hypoxia-inducible factor. EMBO J 2012;31:2448–60.
14. Shabsigh A, Ghafar MA, de la Taille A, Burchardt M, Kaplan SA, Anastasiadis AG, et al. Biomarker analysis demonstrates a hypoxic environment in the castrated rat ventral prostate gland. J Cell Biochem 2001;81:437–44.
15. Halin S, Hammarsten P, Wikstrom P, Bergh A. Androgen-insensitive prostate cancer cells transiently respond to castration treatment when growing in an androgen-dependent prostate environment. Prostate 2007;67:370–7.
16. Park C, Kim Y, Shim M, Lee Y. Hypoxia enhances ligand-occupied androgen receptor activity. Biochem Biophys Res Commun 2012;418:319–23.
17. Mitani T, Harada N, Nakano Y, Inui H, Yamaji R. Coordinated action of hypoxia-inducible factor-1alpha and beta-catenin in androgen receptor signaling. J Biol Chem 2012;287:33594–606.
18. Fernandez EV, Reece KM, Ley AM, Troutman SM, Sissung TM, Price DK, et al. Dual targeting of the androgen receptor and hypoxia-inducible factor 1alpha pathways synergistically inhibits castration-resistant prostate cancer cells. Mol Pharmacol 2015;87:1006–12.
19. Li Y, Alsagabi M, Fan D, Bova GS, Tewfik AH, Dehm SM. Intragenic rearrangement and altered RNA splicing of the androgen receptor in a cell-based model of prostate cancer progression. Cancer Res 2011;71:2108–17.
20. Li Y, Yang R, Henzler CM, Ho Y, Passow C, Auch B, et al. Diverse AR gene rearrangements mediate resistance to androgen receptor inhibitors in metastatic prostate cancer. Clin Cancer Res 2020;26:1965–76.
21. Li Y, Chan SC, Brand LJ, Hwang TH, Silverstein KA, Dehm SM. Androgen receptor splice variants mediate enzalutamide resistance in castration-resistant prostate cancer cell lines. Cancer Res 2013;73:483–9.
22. Young C, Schluep T, Hwang J, Eliasof S. CRLX101 (formerly IT-101)—a novel nanopharmaceutical of camptothecin in clinical development. Curr Bioact Compd 2011;7:8–14.
23. Clark AJ, Wiley DT, Zuckerman JE, Webster P, Chao J, Lin J, et al. CRLX101 nanoparticles localize in human tumors and not in adjacent, nonneoplastic tissue after intravenous dosing. Proc Natl Acad Sci U S A 2016;113:3850–4.
24. Beppu K, Nakamura K, Linehan WM, Rapisarda A, Thiele CJ. Topotecan blocks hypoxia-inducible factor-1alpha and vascular endothelial growth factor expression induced by insulin-like growth factor-I in neuroblastoma cells. Cancer Res 2005;65:4775–81.
25. Rapisarda A, Zalek J, Hollingshead M, Braunschweig T, Uranchimeg B, Bonomi CA, et al. Schedule-dependent inhibition of hypoxia-inducible factor-1alpha protein accumulation, angiogenesis, and tumor growth by topotecan in U251-HRE glioblastoma xenografts. Cancer Res 2004;64:6845–8.
26. Lin CJ, Lin YL, Luh F, Yen Y, Chen RM. Preclinical effects of CRLX101, an investigational camptothecin-containing nanoparticle drug conjugate, on treating glioblastoma multiforme via apoptosis and antiangiogenesis. Oncotarget 2016;7:42408–21.
27. Conley SJ, Baker TL, Burnett JP, Theisen RL, Lazarus D, Peters CG, et al. CRLX101, an investigational camptothecin-containing nanoparticle–drug conjugate, targets cancer stem cells and impedes resistance to antiangiogenic therapy in mouse models of breast cancer. Breast Cancer Res Treat 2015;150:559–67.
28. Pham E, Birrer MJ, Eliasof S, Garmey EG, Lazarus D, Lee CR, et al. Translational impact of nanoparticle–drug conjugate CRLX101 with or without bevacizumab in advanced ovarian cancer. Clin Cancer Res 2015;21:808–18.
29. Pham E, Yin M, Peters CG, Lee CR, Brown D, Xu P, et al. Preclinical efficacy of Bevacizumab with CRLX101, an investigational nanoparticle–drug conjugate, in treatment of metastatic triple-negative breast cancer. Cancer Res 2016;76:4493–503.
30. Markowski MC, Silberstein JL, Eshleman JR, Eisenberger MA, Luo J, Antonarakis ES. Clinical utility of CLIA-grade AR-V7 testing in patients with metastatic castration-resistant prostate cancer. JCO Precis Oncol 2017;2017:PO.17.00127.
31. Lokhandwala PM, Riel SL, Haley L, Lu C, Chen Y, Silberstein J, et al. Analytical validation of androgen receptor splice variant 7 detection in a Clinical Laboratory Improvement Amendments (CLIA) laboratory setting. J Mol Diagn 2017;19:115–25.
32. Font-Tello A, Juanpere N, de Muga S, Lorenzo M, Lorente JA, Fumado L, et al. Association of ERG and TMPRSS2-ERG with grade, stage, and prognosis of

prostate cancer is dependent on their expression levels. Prostate 2015;75:1216–26.
33. Liu C, Lou W, Zhu Y, Nadiminty N, Schwartz CT, Evans CP, et al. Niclosamide inhibits androgen receptor variants expression and overcomes enzalutamide resistance in castration-resistant prostate cancer. Clin Cancer Res 2014;20:3198–210.
34. Liu C, Lou W, Zhu Y, Yang JC, Nadiminty N, Gaikwad NW, et al. Intracrine androgens and AKR1C3 activation confer resistance to enzalutamide in prostate cancer. Cancer Res 2015;75:1413–22.
35. Schluep T, Hwang J, Cheng J, Heidel JD, Bartlett DW, Hollister B, et al. Preclinical efficacy of the camptothecin-polymer conjugate IT-101 in multiple cancer models. Clin Cancer Res 2006;12:1606–14.
36. Liu LL, Xie N, Sun S, Plymate S, Mostaghel E, Dong X. Mechanisms of the androgen receptor splicing in prostate cancer cells. Oncogene 2014;33:3140–50.
37. Moilanen A-M, Riikonen R, Oksala R, Ravanti L, Aho E, Wohlfahrt G, et al. Discovery of ODM-201, a new-generation androgen receptor inhibitor targeting resistance mechanisms to androgen signaling-directed prostate cancer therapies. Sci Rep 2015;5:12007.
38. Luo J, Li Y, Zheng W, Xie N, Shi Y, Long Z, et al. Characterization of a prostate- and prostate cancer-specific circular RNA encoded by the androgen receptor gene. Mol Ther Nucleic Acids 2019;18:916–26.
39. Kregel S, Chen JL, Tom W, Krishnan V, Kach J, Brechka H, et al. Acquired resistance to the second-generation androgen receptor antagonist enzalutamide in castration-resistant prostate cancer. Oncotarget 2016;7:26259–74.
40. Cai C, He HH, Chen S, Coleman I, Wang H, Fang Zi, et al. Androgen receptor gene expression in prostate cancer is directly suppressed by the androgen receptor through recruitment of lysine-specific demethylase 1. Cancer Cell 2011;20:457–71.
41. Cai C, Wang H, Xu Y, Chen S, Balk SP. Reactivation of androgen receptor-regulated TMPRSS2:ERG gene expression in castration-resistant prostate cancer. Cancer Res 2009;69:6027–32.
42. Asangani IA, Wilder-Romans K, Dommeti VL, Krishnamurthy PM, Apel IJ, Escara-Wilke J, et al. BET bromodomain inhibitors enhance efficacy and disrupt resistance to AR antagonists in the treatment of prostate cancer. Mol Cancer Res 2016;14:324–31.
43. Rapisarda A, Uranchimeg B, Sordet O, Pommier Y, Shoemaker RH, Melillo G. Topoisomerase I-mediated inhibition of hypoxia-inducible factor 1: mechanism and therapeutic implications. Cancer Res 2004;64:1475–82.
44. Puc J, Kozbial P, Li W, Tan Y, Liu Z, Suter T, et al. Ligand-dependent enhancer activation regulated by topoisomerase-I activity. Cell 2015;160:367–80.
45. Minelli R, Cavalli R, Ellis L, Pettazzoni P, Trotta F, Ciamporcero E, et al. Nanosponge-encapsulated camptothecin exerts antitumor activity in human prostate cancer cells. Eur J Pharm Sci 2012;47:686–94.
46. Gigliotti CL, Minelli R, Cavalli R, Occhipinti S, Barrera G, Pizzimenti S, et al. *In vitro* and *in vivo* therapeutic evaluation of camptothecin-encapsulated beta-cyclodextrin nanosponges in prostate cancer. J Biomed Nanotechnol 2016;12:114–27.
47. Tian Xi, Nguyen M, Foote HP, Caster JM, Roche KC, Peters CG, et al. CRLX101, a nanoparticle–drug conjugate containing camptothecin, improves rectal cancer chemoradiotherapy by inhibiting DNA repair and HIF1alpha. Cancer Res 2017;77:112–22.
48. Gaur S, Wang Y, Kretzner L, Chen L, Yen T, Wu X, et al. Pharmacodynamic and pharmacogenomic study of the nanoparticle conjugate of camptothecin CRLX101 for the treatment of cancer. Nanomedicine 2014;10:1477–86.
49. Fruehauf JP, Gomez DC, Spitalny L, Kim JH. Topotecan-mediated inhibition of HIF1α/ARV7 heterodimers in 22RV1 prostate cancer cells prevents ARV7 nuclear entry, reversing enzalutamide resistance [abstract]. In: Proceedings of the AACR Annual Meeting 2020; April 27–28 2020 and June 22–24 2020; Philadelphia, PA; 2020. Abstract 4098.
50. Fruehauf JP, Farrokhian N, Sarkissian S, Kim JH. Blockade of ARV7: HIF1alpha heterodimers after topotecan reverses enzalutamide resistance in 22Rv1 cells. J Clin Oncol 2016;34:e16594. https://ascopubs.org/doi/abs/10.1200/JCO.2016.34.15_suppl.e16594.
51. Li Q, Deng Qu, Chao H-P, Liu X, Lu Y, Lin K, et al. Linking prostate cancer cell AR heterogeneity to distinct castration and enzalutamide responses. Nat Commun 2018;9:3600.
52. Mertz KD, Setlur SR, Dhanasekaran SM, Demichelis F, Perner S, Tomlins S, et al. Molecular characterization of TMPRSS2–ERG gene fusion in the NCI-H660 prostate cancer cell line: a new perspective for an old model. Neoplasia 2007;9:200–6.
53. St John J, Powell K, Conley-Lacomb MK, Chinni SR. TMPRSS2-ERG fusion gene expression in prostate tumor cells and its clinical and biological significance in prostate cancer progression. J Cancer Sci Ther 2012;4:94–101.
54. Roche E, Montaudon D, Kayali S, Houede N, Pourquier P. Role of the ERG transcription factor in the resistance of prostate cancer cells to the topoisomerase I inhibitor camptothecin [abstract]. In: Proceedings of the AACR Annual Meeting; 2014 April 5–9; San Diego, CA: AACR; 2014. Abstract nr 3813.
55. Semaan L, Mander N, Cher ML, Chinni SR. TMPRSS2-ERG fusions confer efficacy of enzalutamide in an *in vivo* bone tumor growth model. BMC Cancer 2019;19:972.
56. Grande E, Fernandez Perez MP, Wetterskog D, Font Pous A, Vazquez-Estevez S, Gonzalez del Alba A, et al. A phase II multicenter biomarker trial to study the predictive value of TMPRSS2-ERG before enzalutamide treatment in chemonaïve metastatic castration-resistant prostate cancer. J Clin Oncol 2019;37:5040. https://ascopubs.org/doi/abs/10.1200/JCO.2019.37.15_suppl.5040.
57. Chiang K-C, Tsui Ke-H, Chung Li-C, Yeh C-N, Chang P-L, Chen W-T, et al. Topoisomerase inhibitors modulate gene expression of B-cell translocation gene 2 and prostate specific antigen in prostate carcinoma cells. PLoS ONE 2014;9:e89117.
58. Liu S, Yuan Y, Okumura Y, Shinkai N, Yamauchi H. Camptothecin disrupts androgen receptor signaling and suppresses prostate cancer cell growth. Biochem Biophys Res Commun 2010;394:297–302.
59. Han W, Gao S, Barrett D, Ahmed M, Han D, Macoska JA, et al. Reactivation of androgen receptor-regulated lipid biosynthesis drives the progression of castration-resistant prostate cancer. Oncogene 2018;37:710–21.
60. Zhou CKe, Young D, Yeboah ED, Coburn SB, Tettey Y, Biritwum RB, et al. TMPRSS2:ERG gene fusions in prostate cancer of West African men and a meta-analysis of racial differences. Am J Epidemiol 2017;186:1352–61.